# Data-efficient, Explainable and Safe Payload Manipulation: An Illustration of the Advantages of Physical Priors in Model-Predictive Control

Achkan Salehi<sup>1</sup> and Stephane Doncieux<sup>1</sup>

Abstract—Machine Learning methods, such as those from the Reinforcement Learning (RL) literature, have increasingly been applied to robot control problems. However, such control methods, even when learning environment dynamics (e.g. as in Model-Based RL/control) often remain data-inefficient. Furthermore, the decisions made by learned policies or the estimations made by learned dynamic models -unlike those made by their hand-designed counterparts —are not readily interpretable by a human user without the use of Explainable AI techniques. This has several disadvantages, such as increased difficulty both in debugging and integration in safety-critical systems. On the other hand, in many robotic systems, prior knowledge of environment kinematics and dynamics is at least partially available (e.g. from classical mechanics). Arguably, incorporating such priors to the environment model or decision process can help address the aforementioned problems: it reduces problem complexity and the needs in terms of exploration, while also facilitating the expression of the decisions taken by the agent in terms of physically meaningful entities. Our aim with this paper is to illustrate and support this point of view. We model a payload manipulation problem based on a real robotic system, and show that leveraging prior knowledge about the dynamics of the environment can lead to improved explainability and an increase in both safety and data-efficiency, leading to satisfying generalization properties with less data.

### I. Introduction

Model-based Reinforcement Learning (MBRL) [1], [2] and Model-Predictive Control (MPC) [3], [4], [1] approaches have increasingly been applied to robotic systems. This methods, while displaying similar adaptivity and generalization to Model Free Reinforcement Learning (MFRL) algorithms, have been shown to be superior in terms of data-efficiency, particularly in low-data regimes [5], [6]. This is particularly important on robotic systems, where the large number of interactions required by model-free methods are often impractical.

However, the data-efficiency of MBRL/MPC relative to Model free approaches does not necessarily imply that their are inexpensive. Learning a model of the environment in general requires extensive exploration of the state space, for which random sampling of actions —especially in high-dimensional state-action spaces —is often insufficient [7]. Efficient exploration for both MBRL and MFRL is thus still an active area of research, with proposed solutions using diverse strategies ranging from mutual information maximization [7] to entropy maximization [8] and Quality-Diversity [9].

A second issue which is particularly important in the context of robotics is that the decisions made by learned policies or the estimations made by learned dynamic models are not readily interpretable by a human user without the use of Explainable AI techniques[10].

Both authors are with the ISIR laboratory at Sorbonne University, Paris, France. achkan.salehi@sorbonne-universite.fr, stephane.doncieux@sorbonne-universite.fr

This has several disadvantages, such as increased difficulty both in debugging and integration in safety-critical systems.

On the other hand, in many robotic systems, prior knowledge of environment kinematics and dynamics is at least partially available (e.g. from classical mechanics). Incorporating such priors to the environment model or decision process can help address the aforementioned problems: it should reduces problem complexity and the needs in terms of exploration, while also facilitating the expression of the decisions taken by the agent in terms of physically meaningful entities. We note that the idea of incorporating knowledge inferred from the rules of physic is not new, and has been studied in gray-box system identification [11] and MBRL with gray-box models [12], [13], where it has been shown to present advantages in terms of data-efficiency and safety. Our aim with this paper is to illustrate and further support this point of view in the context of MPC, using a problem from an industrial use-case.

We model a payload manipulation problem based on the SOTO2 (figure 1(a) left), which is manufactured by by Magazino GmbH and deployed in production/assembly lines in order to autonomously manipulate and transport payloads of varying dimensions and mass distributions. In this work, we focus on its gripper, which leverages two independent conveyor belts (figure 1(a) (right)). For reasons tied to storage requirements, it would be desirable to design a controller that would be able to rotate boxes by  $\frac{\pi}{2}$  in a *safe* manner, regardless of their mass distribution.

The solution that we propose is based on deriving a simplified model of the dynamics of the box, and training a neural network to predict its mass distribution using data from a short exploration phase. The predicted mass distribution is then used to compute estimates (e.g. moments of inertia) that are necessary for MPC based control using the equations of motion. We evaluate that approach using a pybullet [14] simulation of the SOTO2's gripper, and show that it has several advantages compared to MPC with a blackbox model. Aside from data-efficiency and better explainability, it also enables us to identify potential hazardous cases and halt the operation, which otherwise could lead to failure and even damaged hardware.

The paper is structured as follows. In the following section (§II), we present a general formalization of our problem of interest, discuss some of the related literature and specify our aims. As a particular case, the box rotation problem discussed above and our physical priors based solution are discussed in §III, and experimental evaluations using our Pybullet simulation of the gripper are presented in section IV. Finally, method limitations and future directions are discussed in §V.

#### II. PROBLEM FORMULATION

We consider decision problems expressed as Multi-Objective Partially Observable Markov Decision Processes (MO-POMDP). Formally, let  $S \subset \mathbb{R}^N$  and  $\mathcal{A} \subset \mathbb{R}^M$  respectively denote the state and action spaces, and  $\mathcal{F}: S \times S \times \mathcal{A} \to [0,1]$  be the transition probability function, *i.e.*  $\mathcal{F}(s',s,a) = P(s'|s,a)$ . Further more, let  $\{R_i(s',s,a)\}_i$  denote a set of reward signals, and define  $\Omega$  as the

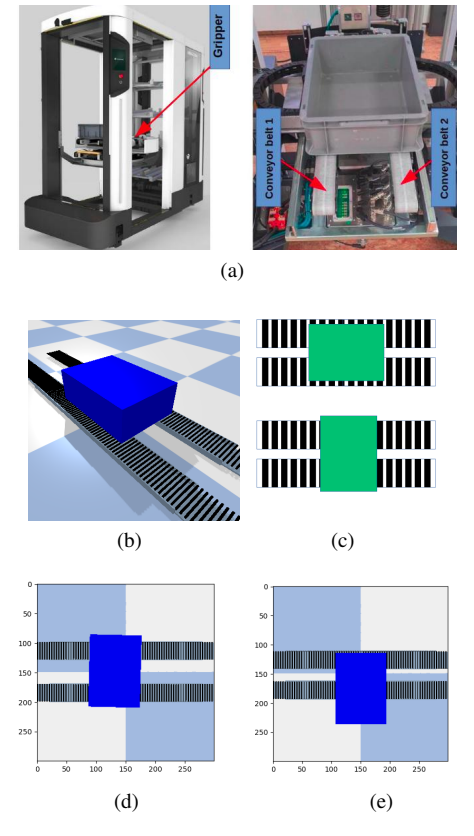


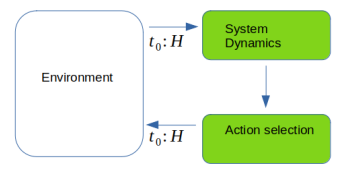
Fig. 1: (a) The SOTO2 robot manufactured by Magazino GmbH, which is deployed in assembly lines (left) and its gripper (right). The gripper is composed of two conveyor belts that can be controlled independently. The motion of beach belt cover is set via velocity controls, and the distance between the two can be adjusted via position control. The aim of a control episode in this work is to rotate boxes of varying and unknown mass distribution by  $\frac{\pi}{2}$ in a safe manner, i.e. the box should either remain well balanced on the conveyors, or manipulation should safely be aborted. (b) An illustration of our pybullet simulation of the gripper, based on roller conveyors. (c, top) Illustration of the initial conditions in each episode. (c, bottom) Target pose that we aim to reach through controlling the conveyor belts. Note that the mass and inertial properties significantly and discontinuously vary in-between episodes. (d) Example final state from a safe rotation, where the box stays well balanced on the conveyors during the episode. Depending on the mass distribution and the center of mass, this can be difficult to achieve, leading to unsafe rotation as shown in (e).

set of possible observations. Then we define an MO-POMDP task as  $\mathcal{T} \triangleq < S, \mathcal{A}, \mathcal{F}, \{R_i\}_i, \Omega, \Phi, \gamma>$ , with  $\gamma \in [0,1]$  a discount factor, and where  $\Phi: S \times \Omega \to [0,1]$  defines the probability  $p(\omega|s)$  of an element  $\omega$  of the observation space  $\Omega$  given a state s. We will note  $\xi_n: \omega_0 \times \omega_1 \times \ldots \times \omega_n \to Z$  the function (learned or hand designed) which maps a history of observations to a state estimation.

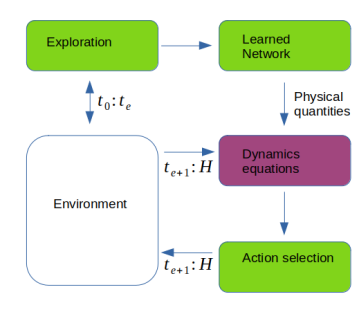
Given two states s,s' and a set of plausible actions  $\{a_1,...,a_l\}$ , each action  $a_j$  will have a corresponding set of rewards  $R_i^j \triangleq R_i(s',s,a_j)$ . As is usual in the multicriteria decision literature, we define the pareto-dominance relationship between actions  $a_j,a_k$  as  $a_j \prec a_k \iff (\exists i \text{ s.t. } R_i^k > R_j^i \text{ and } R_s^k \geq R_s^j \ \forall s)$ . We will say that  $a_k$  pareto dominates  $a_j$  whenever that relation holds. We will define the pareto front at a time step t as the set of all actions that are *not* pareto dominated by any other action at this time, *i.e.*  $A_{front}^t = \{a_j | a_k \not \neq a_k \ \forall k\}$ .

Model Predictive Control Model Predictive Control in general refers to a planning process which uses a learned or known model of environment dynamics to estimate the value of different actions over some time horizon and —often greedily —applies the best ones to the system. The possible mechanisms for action generation and selection range from sampling approaches such as the cross-entropy method [4], [15], [3] and random shooting [6] to training policies [2], [5]. The latter case is often referred to as Model based Reinforcement Learning (MBRL) [1]. Likewise, while some works assume that the model of the environment is known (e.g. the authors of iCEM[4] directly use the simulation as a model), others [15], [3] learn the dynamics of the environment. The majority of works in the MPC/MBRL literature take a blackbox approach to learning environment dynamics (figure 2(a)), often via fitting a function approximator such as a neural network or Gaussian processes to data from the environment.

Leveraging physics to improve MPC. In many robotics systems, standard tools from classical mechanics can be used to -at least partially —describe the dynamics of the system in a symbolic manner, and that prior knowledge can then be incorporated in the MPC or MBRL pipeline (figure 2 (b)). The idea of incorporating knowledge inferred from the rules of physic is not new, and has been studied in grav-box system identification [11], [16] and MBRL with gray-box models [12], [13], where it has been shown to present advantages in terms of data-efficiency and safety. Similarly, such ideas have also been explored in works on physics informed neural networks [17]. Observing that the majority of the MBRL and MPC literature for robotic manipulation is focused on black-box models, our aim in this paper is to present a problem faced by an industrial robot as an illustrative example of the advantages of incorporating priors in MPC pipelines, in particular in terms of safety, data-efficiency and explainability.



(a) Classical model-predictive control with fully learned dynamcis.



(b) Model-predictive control leveraging prior knowledge about the physics of the environment.

Fig. 2: Difference between model-predictive control with a fully learned model and a gray-box model that incorporates prior physical knowledge on the dynamics. The green blocks are those that can be fully or partially learned in each pipeline. The notation  $t_i$ :  $t_j$  indicate the range of timestamps during which an interaction happens, with H denoting the time horizon.

Additional notations. As discussed in the introduction, the particu-

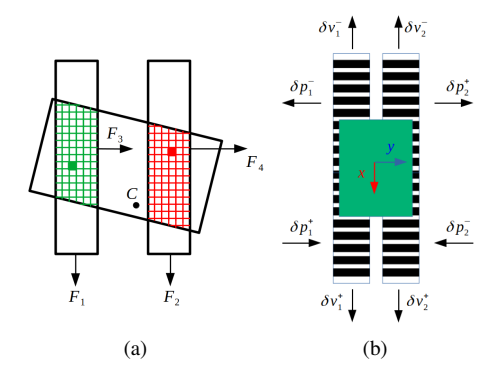


Fig. 3: (a) Top view diagram of the two conveyor belts with illustrative instances of force vectors  $F_i$ . The shaded volumes, which are those that rest on the conveyor belts, are used to compute torque and friction as well as the velocity control to force mapping. They are denoted  $S_1$  (green) and  $S_2$  (red) in the text. (b) A top view illustration of the conveyors with a box on top of them, along with the referential x,y attached to the conveyors. Also shown are the different position and velocity controls. The position controls  $\delta p_i^+, \delta p_i^-$  can move the conveyors closer or apart along the y axis, and the velocity controls  $\delta v_i^+, \delta v_i^-$  move the surface of the conveyors up or down along the x axis. The action space is thus in  $\mathbb{R}^4$ 

lar system that we will focus on consists in using two conveyor belts to rotate boxes with different (a priori unknown) mass distribution. It will be useful for computing physical quantities such as moments of inertia to consider the box as a voxel volume  $\Pi$  with resolution  $N=N_l\times N_w\times N_h$ , effectively considering it as a particle system where the positions of the particles coincide with the center of the voxels. We will note those voxels  $\{Q_1,...,Q_N\}$ . For similar reasons, the delimitation of the area of the box resting on the conveyor belts will be important. Those areas, shown as shaded red and green areas in figure 3(a), will respectively be noted  $S_1, S_2$ . In other terms

$$S_1 = \{Q_i | Q_i \in \Pi \text{ is in direct contact with the left conveyor}\}$$
  
 $S_2 = \{Q_i | Q_i \in \Pi \text{ is in direct contact with the right conveyor}\}.$ 
(1

Given a mass element in a rigid body (or a particle in a particle system), we will note  $r, \dot{r}, \ddot{r}$  respectively its position, velocity and acceleration in world coordinates. When necessary for disambiguation, we will use a subscript, e.g.  $r_{geom}$  for the position of the geometric center,  $r_Q$  for the position of voxel Q, etc. We will often use the position, velocity and acceleration  $r', \dot{r}', \ddot{r}'$  relative to the center of mass  $r_c$ , which is defined as

$$Mr_c = \int rdm \tag{2}$$

which can be considered as a particle at which the entire mass of the body M is concentrated, and whose acceleration under the external force F applied to the body obeys the super-particle theorem:  $M\ddot{r}_c = F$ . We will decompose external forces acting on the box into four component  $F_1,...,F_4$ , which each corresponds to one of the actions (figure 3 (a,b)). Angular velocity will be defined as  $\omega \triangleq \frac{d\phi}{dt} \vec{u}$  with  $\vec{u}$  the rotation axis and  $\phi$  the angle relative to the center of mass. The moments of inertia tensor relative to the center of mass will be noted  $I_c$ . Angular momentum will be written  $H_c$  and  $\tau \triangleq \frac{dH_c}{dt} = I_c\dot{\omega}$  will denote torque. We will also use  $\tau = \int r \times df$  to compute the total torque of the rigid body.

Finally, the projection of vector u on vector v will be denoted  $\mathbf{proj}(u,v) \triangleq \frac{v^T u}{||v||^2} v$ .

# III. CASE STUDY: BOX MANIPULATION USING CONVEYOR BELTS

We consider a payload manipulation problem encountered by the industrial SOTO2 autonomous robot (figure 1(a)), which is manufactured by Magazino GmbH and deployed in production or assembly lines. In some situations it is desirable for the robot to be able to safely rotate boxes by  $\frac{\pi}{2}$  on its gripper, which is composed of two conveyor belts (figure 1(a) right), whose individual rolling motions as well as relative distance can be controlled, respectively via velocity and position control (figure 3(b)), resulting in a 4d control vector. The robot perceives images from the conveyors and the box via an RGBD camera positioned directly above the gripper, with its axis orthogonal to the ground. Its output is processed by standard computer vision algorithms, from which higher-level observations such as the 3d planar pose of the geometric center of the box are available.

In the settings in which the robot operates, the dimensions of the box are known in advance. However, this is not the case for box mass distributions which vary significantly from an episode to the next. The manner in which the box should be rotated depends on the moments of inertia and the center of mass which affects the frictions experienced by the box, and therefore an inadaptive rotation solution (*e.g.* trivially settings the two conveyor belts to roll in opposite directions) can result in poorly balanced, unsafe rotations, as illustrated in figure 1(e). Our aim is to keep the box well balanced during the entire operation, and reach a final state similar to the one from figure 1(d).

We note that safe operation is not possible for all mass distributions. For example, highly skewed mass distributions for which most of the mass falls on one of the conveyor belts are problematic. Such corner-cases constitute an additional motivation for incorporating knowledge about the environment's physics in the control pipeline. Indeed, in the presented problem, estimating the center of mass and moments of inertia can help detect hazardous cases beforehand, which will allow the system to safely abort the manipulation.

Note that a prior paper [3] has used a similar box rotation problem, also based on the SOTO2. However, as further discussed in section  $\S IV$ , their focus is on an unrelated problem, and they only used two degrees of freedom from the gripper, leading to simplified dynamics. In contrast, here, we consider a 4d action space.

Before describing our solution, we first enunciate two assumptions:

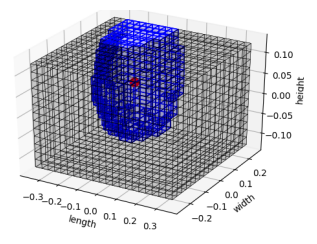
- The mass distribution of the box should not change significantly during an episode.
- 2) The available computer vision pipeline processing the visual input from the robot should provide 3d pose estimation as well as a delimitation of the intersection between the box and the conveyor belts. Both of these tasks can be easily achieved with standard computer vision tools<sup>2</sup>. In our simulated experiments, we directly get those results from the physics engine.

# A. Specifying the MO-POMDP

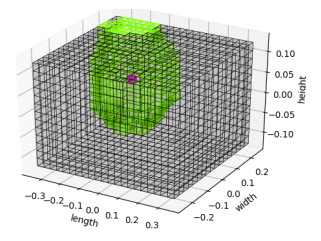
We cast the problem as an MO-POMDP with the components given below.

**Reward functions**. As our aim is to *safely* rotate the box, we define our set  $\{R_i\}$  of objectives as being comprised of two dense reward signals: a pose error reward  $R_1$  and a safety criterion  $R_2$ , which only depend on the state s' that is reached as a result of action a:

<sup>&</sup>lt;sup>2</sup>Indeed, such pipelines are already available on the robot and have been used in previous works [3]



(a) Example of a randomly sampled box mass distribution.



(b) Predicted mass distribution corresponding to the example given in figure 4(a) above. The prediction is made by the learned model based on a short fixed exploratory sequence of commands at the begining of an episode.

Fig. 4: Example of ground truth and estimated mass distribution, which in this work are approximated as a binary occupancy grid and a total mass value M, equally distributed between the occupied cells. In our implementation, a small ( $\sim 0.001$ ) positive value is also added to the mass of each voxel, in order to avoid degenerate cases with zero friction at contact points. Note that the moments of inertia matrix and center of mass are computed based on the predicted mass distribution.

$$R_1(s', s, a) = R_1(s') = (||z_{geom} - z_{target}||_2^2 + \epsilon)^{-1}$$

$$R_2(s', s, a) = R_2(s') = (||r_{geom} - \frac{(P_y^1 + P_y^2)}{2}||_2^2 + \epsilon)^{-1}.$$
(3)

with  $\epsilon \in \mathbb{R}^+$  an infinitesimal value preventing division by zero. In the first equation,  $z_{geom}$  is the orientation of the referential attached to the geometric center of the box, and  $z_{target}$  is the target orientation written in minimal (e.g. Rodrigues) representation. In the second equation,  $P_y^1, P_y^2$  respectively denote the y coordinates (figure 3(b)) at which the left conveyor and right conveyor belts are positioned. In other words, the  $R_2$  function rewards the decision process for centering the geometric center  $r_{geom}$  of the box between the conveyor belts.

**State space** is given by a 5d vector which results from concatenating the position of the conveyors along the y axis (the referential attached to the conveyors is shown in figure 3(b)) to the 3d planar pose of the box.

**Observations** consist of three components: 1) the 3d pose of the geometric center of the box 2) The surface  $S_1$  from the box which intersects the left conveyor, and 3) the surface  $S_2$  of the box which intersects the second conveyor. All of these observations can be provided via standard computer vision algorithms on the real robot, and can be directly retrieved in simulations.

The action space is four dimensional, with two dimensions corresponding to velocity controls setting the rolling motion of the conveyors, and two dimensions setting the position of the conveyors along the y axis (figure 3 )(b)).

# B. Estimating physical priors

As will be discussed in detail in the next subsection, different physical quantities such as the center of mass, moments of inertia and the frictions being applied to  $S_1$  and  $S_2$  have to be estimated. A straight-forward way to enable the estimation of all of these values is to predict the entire mass distribution of the box as a voxel volume, based on an initial short exploration phase.

In this work, we manually defined a short, *fixed* sequence of controls<sup>3</sup>, to be sent to the robot at the beginning of each episode. The trajectory from this initial exploration (composed of successive transitions (s, a, s')) is fed to a small neural network<sup>4</sup>, henceforth noted  $\mathcal{H}$ , which jointly predicts the mass distribution as a 3d occupancy grid and a scalar value as an estimate of the total mass. Figure 4 (a,b) show the ground truth and prediction for a random test mass distribution obtained with our network.

It should be noted that in environments with complex dynamics, learning a black-box model of the environment or learning a Model-Free RL agent requires significant exploration, which is much more costly than the short exploratory phase that the proposed method requires. Another advantage of predicting the mass distribution is that it easily allows us to abort the manipulation early when the detected distribution is physically impossible to safely manipulate.

# C. Physical priors based MPC for box rotation

We will now describe the action evaluation and selection mechanisms after the exploratory phase is over and an estimate of the mass distribution  $\hat{\Pi}$  has become available. At each time step t, we sample actions  $\{a_1^t,...,a_l^t\}$  according to a simple random shooting. The total force F applied to the center of mass as a result of an action  $a_j^t$  is decomposed into four components  $F_1, F_2, F_3, F_4$ , such that  $F_1, F_3$  correspond to forces applied to  $S_1$  and  $F_2, F_4$  are applied to  $S_2$ . Furthermore,  $F_1, F_2$  are aligned with the x axis of the referential attached to the conveyor belts and  $F_3, F_4$  are aligned with its y axis. An example of such a decomposition is given in figure 3(a). In this section, we assume that the mapping  $a_j^t \mapsto \{F_1, F_2, F_3, F_4\}$  between each action and the decomposition of the resulting force is known. The manner in which this mapping is constructed will be discussed in §III-D.

To determine the  $R_i^j$  associated to an action  $a_j^t$ , we predict the next state (timestamp  $t+\delta t$ ) that results from applying  $a_j^t$  to the system. This can be done in the following way. Let us consider the equations of motion[18]: we know that for a given mass element —or voxel —from the box,

$$\ddot{r} = \ddot{r}_c + \dot{\omega} \times r' + \omega \times (\omega \times r')$$

$$\dot{r} = \dot{r}_c + \omega \times r'.$$
(4)

Denoting F the total force that results from action  $a_j^t$  on the center of mass, We can write

<sup>3</sup>The sequence, applied for 45 consecutive timesteps, was comprised of 15 control vectors, with each action repeated three times. The 15 control vectors were chosen manually, and correspond to the commands necessary to apply a small rotation and translation to a box of uniform mass.

 $^4\mathrm{The}$  network is composed of a backbone of a few fully connected layers followed by two heads, one for predicting an occupancy grid to approximate the distribution, and another to predict a single scalar for total mass. The network is trained end to end using the Adam optimizer, with a loss given as a linear combination between a Binary Cross-entropy (BCE) loss computed on the occupancy grid output by the first head, and an MSE loss taking as input the scalar output of the second head. As the network has  $\sim 2e6$  parameters, training an inference are easily performed on CPU.

 $^5$ The random shooting process used here is simple: each dimension of the action space is discretized, and at each time step,  $N_a$  actions are selected among all the possible vectors formed by this discretization. In this work, discretization resulted in 95 actions, and we set  $N_a = 50$ .

$$\ddot{r}_c(t) \approx {}_0 \ddot{r}_c(t) + {}_F \ddot{r}_c + \beta \tag{5}$$

where  $_0\ddot{r}_c(t)$  is the acceleration of the center of mass without the application of  $a_j^t$ . Note that the observations produced by the computer vision pipeline include the pose  $r_{geom}$  of the geometric center of the box, and that an estimation of its position relative to  $r_c$  is available from  $\hat{\Pi}$ . Therefore,  $_0\ddot{r}_c(t)$  can be approximated in a straight-forward manner from a sliding window of observations. The term  $_F\ddot{r}_c$  is the acceleration that results from applying  $a_j^t$  and thus F to the system, and it can easily be recovered from the relation  $M\ddot{r}_c = F$ . The term  $\beta$  is a correction term that will be computed later based on estimated frictions.

We recover the angular acceleration from the relation

$$\dot{\omega} = I_c^{-1} \tau. \tag{6}$$

In order to estimate  $\tau$ , we leverage the observations  $S_1$  and  $S_2$  (defined via equation 1):

$$\tau = \sum_{Q \in \hat{\Pi}} r'_Q \times \delta F^Q$$

$$= \sum_{Q \in S_1} r'_Q \times \delta F^Q + \sum_{Q \in S_2} r'_Q \times \delta F^Q$$

$$= \sum_{Q \in S_1} r'_Q \times (\delta F_1^Q + \delta F_3^Q) + \sum_{Q \in S_2} r'_Q \times (\delta F_2^Q + \delta F_4^Q)$$
(7)

where  $\delta F_Q$  is the force applied to voxel Q, and

$$\begin{cases} \delta F_i^Q \approx \frac{F_i}{|S_1|} & i \in \{1,3\} \\ \delta F_i^Q \approx \frac{F_i}{|S_2|} & i \in \{2,4\}. \end{cases}$$
 (8)

Note that the position of the geometric center of the box,  $r_{geom}$ , is observed via the computer vision pipeline, and since its relative distance from  $r_c$  is known from the estimated mass distribution  $\hat{\Pi}$ , we can compute  $r_Q'$  for all voxels Q. Similarly,  $I_c$  can be trivially computed from  $\hat{\Pi}$ . Plugging this value and the computed  $\tau$  into equation 6 allows us to recover  $\hat{\omega}$ . As for  $\omega$  itself, we can approximate it as  $\omega \approx \frac{r_Q'(t) - r_Q'(t - \delta t)}{\delta t}$  using any voxel Q, as long as it does not coincide with the center of mass. Similarly,  $\hat{r}_c \approx \frac{r_c(t) - r_c(t - \delta t)}{dt}$ .

We now have estimates for all the unknowns of equations 4 and 5 except for  $\beta$ . For now, we make a first prediction without accounting for frictions:

$$\hat{r}^{\text{frictionless}}(t+\delta t) = r(t) + \dot{r}(t)\delta t + \frac{1}{2}(\ddot{r}(t)-\beta)\delta t^2 \qquad (9)$$

In order to estimate the frictions, we consider the current and predicted motion of each voxel on the  $S_i$ . The action  $a_j^t$  results in a friction that is in the direction opposite to  $\delta \hat{r}(t+\delta t) \triangleq \hat{r}^{frictionless}(t+\delta t) - r(t)$ . Note however that the friction that the voxel Q experiences before  $a_j^t$  is applied, and which is in the direction opposite to  $\dot{r}_Q(t)$ , is already accounted for in  $\ddot{r}_Q(t)$ . Thus, we are only interested in the additional friction component orthogonal to the latter. Noting  $\eta_Q^f$  the direction of this friction, we have

$$\eta_O^f = -\delta \hat{r}(t + \delta t) - \mathbf{proj} \left( -\delta \hat{r}(t + \delta t), -\dot{r} \right) \tag{10}$$

Let us now define the volume  $V_1$  as a superset of  $S_1$ :

$$\mathcal{V}_1 \triangleq \{Q \in \hat{\Pi} | Q \in S_1 \text{ or } Q \text{ is above the voxels of } S_1.\}.$$
 (11)

In other terms,  $V_1$  is the set of voxels lying on the left conveyor belt, but unlike those included in  $S_1$ , they are not required to

directly touch the conveyor. The volume  $V_2$  is defined analogously. With that notation, the total friction is given by

$$F_f = \sum_{i \in \{1,2\}} \sum_{Q \in \mathcal{V}(S_i)} \eta_Q^f . \mu_k . g. dM^Q$$
 (12)

where  $\mu_k$  is the kinetic friction coefficient,  $g\approx 9.8$  and  $dM^Q$  is the mass value associated to Q. This mass is known from the predicted mass distribution  $\hat{\Pi}$ . The correction term  $\beta$  can now be computed as  $\beta=\frac{F_f}{M}$  and plugged into equation 5. Similar corrections can be applied to the torque.

The final form of the prediction will then be given by

$$\hat{r}(t+\delta t) = r(t) + \dot{r}(t)\delta t + \frac{1}{2}\ddot{r}(t)\delta t^2.$$
 (13)

In particular, this allows us to predict  $r_{geom}$ , which is the only quantity that the safety reward  $R_2$  depends on. However, we also need to predict an orientation to compute the pose reward  $R_1$ . Since we are only interested in the planar motion of the box, orientation is reduced to a single angle  $\theta_{geom}$ . Analogously to the derivations above, this can be done by considering the Taylor expansion  $\hat{\theta}_{geom}(t+\delta t)=\theta_{geom}(t)+\omega\delta t+\frac{1}{2}\dot{\omega}\delta t^2$ .

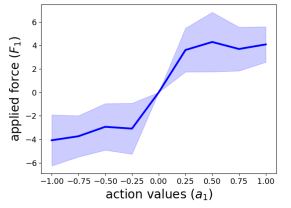
**Action selection.** The action evaluation process above results in a pair  $(R_1(a_j^t), R_2(a_j^t))$  of scores for each of the sampled l actions. The set of potential solutions is given by the pareto front  $A_{front}^t$ . However, the solutions in this set are not comparable, and each represent a different compromise between the two  $R_i$ , that is, between safety and accomplishing the goal. While different selection strategies, ranging from linearly combining the criteria to Choquet integrals [19] were considered, we found that randomly selecting an element from  $A_{front}^t$  lead to satisfactory results.

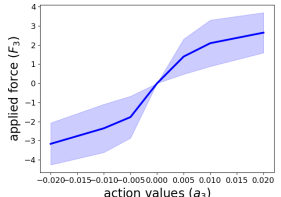
# D. Mapping controls to forces

The framework that we have presented assumes that the mapping  $a \mapsto \{F_1, F_2, F_3, F_4\}$  is known in advance. As in most commercially available robots, the inner workings of the motion control software applying those given commands to joints is often not exposed to the user or easily accessible, we instead use a simple offline "calibration" phase, which uses data gathered from a few short episodes with a box of uniform mass distribution. Controls are sampled randomly but in a disjoint manner, i.e. at each timestep, the 4d sampled action vector should only have a single non-zero component. This is because our aim is to map actions of the form  $a = (a^{1}, 0, 0, 0), a = (0, a^{2}, 0, 0)$  (corresponding to velocity controls  $\delta v$  in figure 3) respectively to  $F_1$  and  $F_2$ , and actions of the form  $a = (0, 0, a^3, 0)$  and  $a = (0, 0, 0, a^4)$  (corresponding to the position controls  $\delta p$  in figure 3) to  $F_3$  and  $F_4$ , respectively. At the end of each trajectory, the acceleration and velocity of each voxel as well as the friction forces are estimated in a manner similar to that of equations 10, 11, 12 above. Assuming that the change of motion at timestamp t is due to the most recently applied action, we can estimate the corresponding force as  $F(a) = M\delta \ddot{r}_c - F_f^1 - F_f^2$  where  $F_f^1$  and  $F_f^2$  are the frictions experienced by  $S_1$  and  $S_2$ . Figures 5 (a, b) show examples of a mapping constructed in this manner using  $\sim 400$  transitions for forces  $F_1$  and  $F_3$ . It can be seen that this mapping is indeed uncertain. In this work, we map each action to the mean value of this mapping, and leave the incorporation of uncertainty to the future.

### IV. EMPIRICAL RESULTS

We evaluate the proposed approach in a simulation developed in Pybullet [14] with rolling conveyor belts [20]. A screenshot of the simulation is given in figure 1(b). Varying mass distributions are generated using 3d gaussians (with dense covariances) approximated as voxel volumes, examples of which have already been shown in figure 4. We note that a similar simulation, but with





- (a) Mapping obtained between velocity controls applied to the  $F_1$ . The map between velocity controls applied to the right is similar.
- (b) Mapping obtained between velocity controls applied to the left hand side conveyor belt and left hand side conveyor belt and  $F_3$ . The map between velocity controls applied to the right hand side conveyor belt and  $F_2$  hand side conveyor belt and  $F_4$ is similar.

Fig. 5: Mappings obtained between applied velocity controls to the different  $F_i$ .

simpler dynamics and different objectives has been used in a prior paper [3]. Two major differences between the two works exits. First, the focus of their work is entirely different from ours: while our aim is to provide a data-efficient, safe and explainable solution, their main objective is to solve issues related to irregular/asynchronous actions/observations. Second, the conveyor belts that they consider have only two degrees of freedom, leading to much simpler system dynamics. While the rolling motion of the surface of the conveyors and their position along the y axis are controlled by our system, theirs only handles the former.

In what follows, we first compare the proposed approach to a classical baseline on four different distributions. Following the analysis of those results, we further validate the proposed approach on 30 other distributions, in particular in terms of safe manipulation.

In order to reduce the complexity of the dynamics and in particular facilitate learning for the baseline, we restricted the actions by only allowing actions of the form  $a = (a_1, a_2, 0, 0)$ ,  $a = (0, 0, a_3, 0)$  or  $a = (0, 0, 0, a_4)$ . That is, we decoupled the application of velocity controls from position controls, and forbade the simultaneous adjustment of the positions  $P_y^1, P_y^2$  of the conveyor belts. These restriction, which we imposed on experiments with both methods, had no incidence on the ability to control the

The mass distribution prediction network  ${\cal H}$  that was used in all experiment was trained on short exploratory phases and thus limited data from 2000 randomly generated boxes (training details are given in table II).

# A. Comparison to a classical baseline.

We consider a classical MPC method using a black-box model of the form  $\hat{s}_{t+1} = \mathcal{W}(s_t, a_t)$  with  $\mathcal{W}$  a small fully connected neural network 6. First, the network is trained using data from several episodes until it reaches satisfactory accuracy. Then, the MPC control method, similar to the proposed approach, uses random shooting for generating actions and assigns  $R_1, R_2$  scores to them based to the next predicted state. However, instead of using the equations of motion, it uses the trained W.

Four different distributions, illustrated in figures 6(a,b,c,d), were used. In what follows, we will refer to them with the labels given to them in the figure, i.e. as distributions A, B, C, D. Note that each conveyor belt simulation instance is defined by the choice of box mass distribution. Distribution A was randomly generated, and its corresponding environment used to train W. Distribution B was manually selected in order to be similar to A, so that we could expect that  $\mathcal{W}$  would generalize reasonably well to this

environment. Distribution C was also picked manually, to ensure that it was sufficiently different from A. Finally, distribution D was selected as an example of distributions that are hazardous and in some cases impossible to safely manipulate, as the entire mass, depending on box position, could entirely fall on one of the conveyor belts.

We found that learning W to reach sufficient accuracy on distribution A was not possible using only data from random policies. Thus, in addition to those, we used data from trajectories obtained from already successful policies (from the physical priors pipeline). Details of the data used for training W are summarized in the second row of table I. These results hint that the proposed approach is indeed less demanding in terms of exploration, and is more data-efficient.

Using the trained  $\mathcal{H}$  and  $\mathcal{W}$  networks, we executed each of the two pipelines 5 times on each of the environments corresponding to the four distributions A, B, C, D. The results are summarized in table II. A notable difference is that W requires online adaptation, especially when the mass distribution is different from the one it has been trained on. We found that updating the model for one epoch (on all data from the current episode) every 20 steps resulted in satisfying performance. The proposed approach, on the other hand, explicitly decouples the physical rules and relations that are common to all seen and unseen tasks from those that only hold in a particular environment. This allows it to be trained on multiple environments (as specified in table I) an generalize in zeroshot manner, while classical blackbox models such as  $\mathcal W$  overfit a single environment. Indeed, one could improve the generalization W through methods such as optimization based meta-learning [21], [22], however, this would exponentially increase the need in terms of data collection.

Both methods have a perfect success rate for distributions A and B. However, as expected from the previous paragraph, the success rate of the baseline drastically falls on distribution C, which unlike distribution B, is highly dissimilar to distribution A.

Adding prior information inferred from physics results in the prediction of meaningful physical quantities, and this interpretability, among other benefits, enables straight-forward implementation of sanity check and safety protocols. Distribution D clearly illustrates that: while MPC using W blindly tries to apply controls to this hazardous configuration, the prior-based method is able to abort execution as the predicted distribution is identified as unsafe.

Before closing this subsection, we note that the baseline outperforms the proposed approach in terms of numbers of timesteps required to solve the task. While we conjecture that this is due to the uncertainty from the  $a \mapsto \{F_1, F_2, F_3, F_4\}$  mapping, we find it also important to emphasize that this lower number of timesteps does not translate to less time-consuming episodes: indeed, the time spend on the frequent on-line updates that are required by W outweighs any gains from the reduced number of timestamps.

# B. Validation on random distributions and safe manipulation We further validate the proposed approach, in particular in terms

of safety, by evaluating its performance on 30 different mass distributions. Two criteria are of importance in defining safety in the box rotation problems: 1) The evolution of the *balance error*  $err_{balance} = ||r_{geom} - \frac{(P_y^1 + P_y^2)}{2}||_2^2$ , which indicates how well  $r_{geom}$  is centered between the two conveyors, and 2) whether the method is capable of aborting the manipulation early (i.e. at the end of the exploration phase) for mass distributions that are physically hazardous to rotate. For the first criterion, based on the real robot, a hard threshold of  $0.1 \times box\_length$  is considered as the safety limit. Given that the boxes used in these experiments are approximately of dimensions  $40cms \times 30cms \times 15cms$  (length, width, height), this corresponds to 4.0cms. For the second criterion, it is first important to define what we mean by hazardous when talking about distributions. Let us note the box as a volume  $([0, l_{box}] \times [0, w_{box}] \times$  $[0, h_{box}]$  with  $l_{box}, w_{box}, h_{box}$  the length, width and height of the

<sup>&</sup>lt;sup>6</sup>The network we considered had  $\sim 2.5e6$  parameters

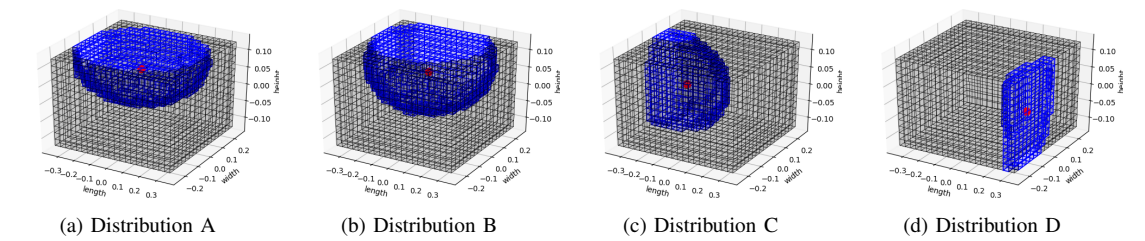


Fig. 6: Different mass distributions (referred to as Distributions A,B,C,D in the text) used in the first set of experiments, in order to compare the proposed method with a classical MPC baseline. (a) The mass distribution on which the MPC baseline is trained. (b) A mass distribution similar to distribution A, for which we expect reasonable generalization from the baseline. (c) A distribution whose difference with distribution A is more pronounced. (d) This heavily skewed mass distribution, which we couple with a mass value of 4.0kg can be considered *uncontrollable* in a safe manner, as all of its mass will fall on one conveyor, resulting in important imbalance in terms of frictions. We *do not* expect either method to succeed in rotating the box without the box becoming dangerously imbalanced during manipulation. However, the proposed method presents an advantage in this case: as it predicts the center of mass, detecting such potentially unsafe cases and aborting the manipulation is straight-forward.

|                                      | num necessary transitions | data from   | zero-shot generalization |  |
|--------------------------------------|---------------------------|---|--------------------------|--|
| Model for physical priors estimation | ∼ 90k                     | 2000 different random boxes                                 | Yes                      |  |
|                                      |                           | (45 fixed initial exploratory steps for each)               |                          |  |
| Model from MPC (baseline)            | ~ 122k                    | data from $\sim 200$ full episodes in a single environment, |                          |  |
|                                      |                           | using random exploration +                                  | No                       |  |
|                                      |                           | known successful policies                                   |                          |  |

TABLE I: Summary of the data used for training the baseline and the model used to predict physical priors.

|  | success ratio | online adaptation             | average number of steps spent in environment |
|--|---------------|-------------------------------|--|
| distribution A, Physical priors based method | 100%          | None                          | 238.8  |
| distribution A, Classical MPC (baseline)     | 100%          | 1 epoch every 20 steps        | 367.4  |
| distribution B, Physical priors based method | 100%          | None                          | 389.2  |
| distribution B, Classical MPC (baseline)     | 100%          | 1 epoch every 20 steps        | 269.6  |
| distribution C, Physical priors based method | 100%          | None                          | 527.8  |
| distribution C, Classical MPC (baseline)     | 60%           | 1 epoch every 20 steps        | 401.0  |
| distribution D, Physical priors based method | Abo           | rts execution as an unsafe of | listribution is detected                     |
| distribution D, Classical MPC (baseline)     | 0%            | 1 epoch every 20 steps        | N.A  |

TABLE II: Results of both methods on the four distributions of figure 6, averaged over five executions per distribution and method. Statistics for which the physics prior based pipeline yields better values are highlighted in green, and those were it was outperformed by the baseline are highlighted in red. We conjecture that the latter are mainly due to the uncertainty in the  $a \mapsto \{F_1, F_2, F_3, F_4\}$  mapping. We Note that contrary to the baseline, the proposed approach operates in a zero-shot manner in each environment, *i.e.* it is not adapted to each new mass distribution.

box, and let us partition the length and width in four equal parts:  $\{[0,\frac{l_{box}}{4}],[\frac{l_{box}}{4},\frac{l_{box}}{4}],[\frac{l_{box}}{2}],[\frac{l_{box}}{2},3\frac{l_{box}}{4}],[3\frac{l_{box}}{4},l_{box}]\}$  and similarly for the width. We will say that

A box mass distribution is *hazardous* to rotate if its entire mass is concentrated in one of those volumes:

$$U_{1} \triangleq [0, \frac{l_{box}}{4}] \times [0, w_{box}] \times [0, h_{box}]$$

$$U_{2} \triangleq [3\frac{l_{box}}{4}, l_{box}] \times [0, w_{box}] \times [0, h_{box}]$$

$$U_{3} \triangleq [0, l_{box}] \times [0, \frac{w_{box}}{4}] \times [0, h_{box}]$$

$$U_{4} \triangleq [0, l_{box}] \times [3\frac{w_{box}}{4}, w_{box}] \times [0, h_{box}].$$
(14)

For these experiments, we randomly sampled 30 mass distributions that were *non-hazardous*. On those environments, the proposed method yielded a success rate of 83.33% (i.e. 25 successes out of 30). Figure 7 summarizes the safety error  $err_{balance}$  obtained with the proposed method. Two points are worth mentioning: first, one failure was due to an incorrect classification of one of the boxes as hazardous as a result of an inaccurate prediction  $\hat{\Pi}$  for that environment. A second failure, also due to an inaccurate  $\hat{\Pi}$  prediction, produces the maximum error shown as the dashed red curve in figure 7. The remaining three failure cases did not suffer from poor mass distribution predictions. We conjecture that failure

in that case is caused by the uncertainties in the mapping  $a \mapsto \{F_1, F_2, F_3, F_4\}$ , which our method does not take into account. Note that the quality of the prediction  $\hat{\Pi}$  was evaluated using the Intersection of Union between the prediction and the ground truth volume.

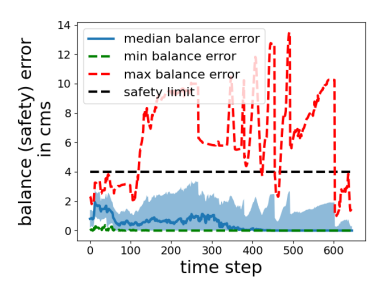


Fig. 7: Balance score obtained on the 30 non-hazardous mass distributions. The shaded area corresponds to one standard deviation around the median. Note that the maximum error (dashed red lines) is caused by an inaccurate prediction from  $\hat{\Pi}$ .

#### V. DISCUSSION AND CONCLUSION

The previous section, based on experiments performed in simulation showed that incorporating priors derived from physics has several benefits: (i) it leads to better data-efficiency due to lowered exploration needs, (ii) enables better generalization through explicitly specifying a subset of rules that are common to all unseen tasks, thus lowering overfitting risks, (iii) is more easily interpretable/explainable and finally, (iv) allows the straight-forward implementation for some safety requirements. Here, we discuss a few remaining questions and future directions. First, we observe that the physical priors were manually identified and provided to the system. This requires more development effort compared to training a black-box method, and is an error-prone process. Thus, one direction that we think is worth exploring in the future is the automatic extraction of such physical priors, using for example large language models or more generally foundation models[23]. Second, estimating physical priors requires less exploration than what is necessary to obtain a full model. However, it should still be sufficiently informative. In the solution we provided to the box rotation problem, we simply used a small manually set fixed sequence of actions. This approach is clearly not optimal for more complex problems. Several directions can be explored, such as learning a dedicated exploration agent through meta-learning, where the reward signal at each meta iteration would depend on the accuracy of the physical prior estimates. Finally, we consider the question of integrating the proposed box rotation solution on the real robot. A possible approach would be to directly train the networks using data from the real robot. In fact, environment models based on Neural ODEs have already been directly trained on the SOTO robot in previous work [3]. However, ensuring the adaptivity of such models to unseen tasks requires ten of thousands of episodes, using approaches such as optimization based meta-learning [3] which is far more expensive than estimating the priors with the physical priors based approach proposed here. That being said, a downside of the proposed method is that it requires knowledge of mass distributions during training. This necessitate the design and manufacture of specific mass distributions for training (e.g. using 3d printed blocks). It thus trades off efforts spent on setting up the experimental platform for data collection and computation time. A more balanced solution in terms of cost would be to combine the use of sim2real methods leveraging techniques such as domain randomization [24], [25], [26] with limited data from the real robot.

# **ACKNOWLEDGMENT**

This work was supported by the European Union's H2020-EU.1.2.2 Research and Innovation Program through FET Project VeriDream (Grant Agreement No. 951992). We wish to thank Quentin Levent for their initial work on the conveyor belt simulation. We express our gratitude to Kathia Melbouci for their valuable input during the development of the presented material.

#### REFERENCES

- T. M. Moerland, J. Broekens, and C. M. Jonker, "Model-based reinforcement learning: A survey," arXiv preprint arXiv:2006.16712, 2020.
- [2] M. Deisenroth and C. E. Rasmussen, "Pilco: A model-based and data-efficient approach to policy search," in *Proceedings of the 28th International Conference on machine learning (ICML-11)*, 2011, pp. 465–472
- [3] A. Salehi, S. Rühl, and S. Doncieux, "Adaptive asynchronous control using meta-learned neural ordinary differential equations," arXiv preprint arXiv:2207.12062, 2022.
- [4] C. Pinneri, S. Sawant, S. Blaes, J. Achterhold, J. Stueckler, M. Rolinek, and G. Martius, "Sample-efficient cross-entropy method for real-time planning," in *Conference on Robot Learning*. PMLR, 2021, pp. 1049– 1065.

- [5] L. Kaiser, M. Babaeizadeh, P. Milos, B. Osinski, R. H. Campbell, K. Czechowski, D. Erhan, C. Finn, P. Kozakowski, S. Levine, et al., "Model-based reinforcement learning for atari," arXiv preprint arXiv:1903.00374, 2019.
- [6] A. Nagabandi, G. Kahn, R. S. Fearing, and S. Levine, "Neural network dynamics for model-based deep reinforcement learning with modelfree fine-tuning," in 2018 IEEE International Conference on Robotics and Automation (ICRA). IEEE, 2018, pp. 7559–7566.
- [7] R. Sekar, O. Rybkin, K. Daniilidis, P. Abbeel, D. Hafner, and D. Pathak, "Planning to explore via self-supervised world models," in *International Conference on Machine Learning*. PMLR, 2020, pp. 8583–8592.
- [8] Y. Seo, L. Chen, J. Shin, H. Lee, P. Abbeel, and K. Lee, "State entropy maximization with random encoders for efficient exploration," in *International Conference on Machine Learning*. PMLR, 2021, pp. 9443–9454
- [9] B. Lim, L. Grillotti, L. Bernasconi, and A. Cully, "Dynamics-aware quality-diversity for efficient learning of skill repertoires," in 2022 International Conference on Robotics and Automation (ICRA). IEEE, 2022, pp. 5360–5366.
- [10] S. R. Islam, W. Eberle, S. K. Ghafoor, and M. Ahmed, "Explainable artificial intelligence approaches: A survey," arXiv preprint arXiv:2101.09429, 2021.
- [11] L. Ljung, System Identification, 2017. [Online]. Available: https://onlinelibrary.wiley.com/doi/abs/10.1002/047134608X.W1046.pub2
- [12] S. K. Chalup, C. L. Murch, and M. J. Quinlan, "Machine learning with aibo robots in the four-legged league of robocup," *IEEE Transactions* on Systems, Man, and Cybernetics, Part C (Applications and Reviews), vol. 37, no. 3, pp. 297–310, 2007.
- [13] M. Lutter, J. Silberbauer, J. Watson, and J. Peters, "Differentiable physics models for real-world offline model-based reinforcement learning," in 2021 IEEE International Conference on Robotics and Automation (ICRA). IEEE, 2021, pp. 4163–4170.
- [14] E. Coumans and Y. Bai, "Pybullet, a python module for physics simulation for games, robotics and machine learning," http://pybullet.org, 2016–2021.
- [15] K. Chua, R. Calandra, R. McAllister, and S. Levine, "Deep reinforcement learning in a handful of trials using probabilistic dynamics models," *Advances in neural information processing systems*, vol. 31, 2018
- [16] S. L. Brunton, J. L. Proctor, and J. N. Kutz, "Sparse identification of nonlinear dynamics with control (sindyc)," *IFAC-PapersOnLine*, vol. 49, no. 18, pp. 710–715, 2016.
- [17] S. Sanyal and K. Roy, "Ramp-net: A robust adaptive mpc for quadrotors via physics-informed neural network," arXiv preprint arXiv:2209.09025, 2022.
- [18] J. L. Meriam, L. G. Kraige, and J. N. Bolton, Engineering mechanics: dynamics. John Wiley & Sons, 2020.
   [19] L. Montaño Guzmán, "Fuzzy measures and integrals," Acta Nova,
- [19] L. Montaño Guzmán, "Fuzzy measures and integrals," Acta Nova, vol. 2, no. 2, pp. 216–227, 2003.
- [20] P. M. McGuire, Conveyors: application, selection, and integration. CRC Press, 2009.
- [21] T. Hospedales, A. Antoniou, P. Micaelli, and A. Storkey, "Meta-learning in neural networks: A survey," *IEEE transactions on pattern analysis and machine intelligence*, vol. 44, no. 9, pp. 5149–5169, 2021.
- [22] X. Song, W. Gao, Y. Yang, K. Choromanski, A. Pacchiano, and Y. Tang, "Es-maml: Simple hessian-free meta learning," arXiv preprint arXiv:1910.01215, 2019.
- [23] R. Bommasani, D. A. Hudson, E. Adeli, R. Altman, S. Arora, S. von Arx, M. S. Bernstein, J. Bohg, A. Bosselut, E. Brunskill, et al., "On the opportunities and risks of foundation models," arXiv preprint arXiv:2108.07258, 2021.
- [24] T. Chaffre, J. Moras, A. Chan-Hon-Tong, and J. Marzat, "Sim-to-real transfer with incremental environment complexity for reinforcement learning of depth-based robot navigation," arXiv preprint arXiv:2004.14684, 2020.
- [25] P. Nikdel, R. Vaughan, and M. Chen, "Lbgp: Learning based goal planning for autonomous following in front," in 2021 IEEE International Conference on Robotics and Automation (ICRA). IEEE, 2021, pp. 3140–3146.
- [26] W. Zhao, J. P. Queralta, and T. Westerlund, "Sim-to-real transfer in deep reinforcement learning for robotics: a survey," in 2020 IEEE Symposium Series on Computational Intelligence (SSCI). IEEE, 2020, pp. 737–744.